REPORT DOCUMENTATION PAGE

Form Approved
OMB No. 0704-0188

1. REPORT DATE (DD-MM-YYYY) 16-12-2003	2. REPORT TYPE Technical Paper	3. DATES COVERED (From - To)

4. TITLE AND SUBTITLE

The Effects of Pressure and Acoustic Field on a Cryogenic Coaxial Jet

5a. CONTRACT NUMBER
F04611-99-C-0025

5b. GRANT NUMBER

5c. PROGRAM ELEMENT NUMBER

6. AUTHOR(S)

D. Davis and B. Chehroudi (ERC, Inc.)

5d. PROJECT NUMBER
2308

5e. TASK NUMBER
M13C

5f. WORK UNIT NUMBER

7. PERFORMING ORGANIZATION NAME(S) AND ADDRESS(ES)

Engineering Research Corporation (ERC), Inc.
10 E. Saturn Blvd.
Edwards AFB CA 93524-7680

8. PERFORMING ORGANIZATION REPORT NUMBER

9. SPONSORING / MONITORING AGENCY NAME(S) AND ADDRESS(ES)

Air Force Research Laboratory (AFMC)
AFRL/PRS
5 Pollux Drive
Edwards AFB CA 93524-7048

10. SPONSOR/MONITOR'S ACRONYM(S)

11. SPONSOR/MONITOR'S NUMBER(S)
AFRL-PR-ED-TP-2003-325

12. DISTRIBUTION / AVAILABILITY STATEMENT

Approved for public release; distribution unlimited.

13. SUPPLEMENTARY NOTES
For presentation at the 42nd AIAA Aerospace Sciences Meeting and Exhibit in Reno, NV, taking place 5-8 January 2004.

14. ABSTRACT

20040123 065

15. SUBJECT TERMS

16. SECURITY CLASSIFICATION OF:			17. LIMITATION OF ABSTRACT	18. NUMBER OF PAGES	19a. NAME OF RESPONSIBLE PERSON Leilani Richardson
a. REPORT Unclassified	**b. ABSTRACT** Unclassified	**c. THIS PAGE** Unclassified	A	21	19b. TELEPHONE NUMBER (include area code) (661) 275-5015

Standard Form 298 (Rev. 8-98)
Prescribed by ANSI Std. 239.18

THE EFFECTS OF PRESSURE AND ACOUSTIC FIELD ON A
CRYOGENIC COAXIAL JET

D. Davis and B. Chehroudi[*]

Engineering Research Corporation, Inc.
10 E. Saturn Boulevard
Edwards AFB, CA 93524-7680
*ChehroudiB@aol.com(Corresponding author)

ABSTRACT

A coaxial injector was designed to inject liquid nitrogen (LN2) with a coflow of gaseous nitrogen (GN2) in its annular region as part of a program to better understand the nature of the interaction between acoustic waves and liquid fuel jets in cryogenic rocket engines. Backlit images were taken from the jets at various flow rates and at sub-, near-, and super-critical chamber pressures with and without the presence of a 2700 Hz standing wave acoustic field. Injector exit plane temperature measurements were made in both the center jet and annular regions. Results indicate that when the jet core appeared short and "thin", mostly under supercritical chamber pressures, the jet became insensitive to the external acoustic field. The strongest interaction was observed when the jet core looked long and "thick". To explore their implications, the characteristic acoustic impedance of the central jet and fuel/oxidizer momentum ratios are considered to play a role in the observed interactions. It is feasible that they play a similar role in cryogenic rocket engine combustion instability of the coaxial jet.

INTRODUCTION

Coaxial type injectors have been used in liquid rocket engines since the 1940's and are found in the present day hardware such as the Space Shuttle Main Engine (SSME), see Hulka and Hutt[1]. Rocket engines such as the SSME use liquid oxygen (LOX) and hydrogen (H_2) as propellants with the LOX flowing through an inner tube (or the center post) of a coaxial injector design, and H_2 through the outer annular region. The two streams undergo jet breakup and mixing processes in the shear layer between the two streams after they exit the injector. Subsequently, combustion and heat release occurs to produce the desired engine thrust.

Often the combustion processes are controlled by, or at least intimately related to, the jet breakup and mixing of the oxidizer and fuel streams. These processes can safely and inexpensively be studied using chemically-inert fuel and oxidizer simulants. Often, parameters such as velocity ratio, mass ratio, density ratio,

Reynolds number (Re), Weber number (We), Ohnesorge number (Oh), etc., are scaled to those of the real engine. The scaling allows reasonable comparisons and evaluation of different injector designs before ever being tested under hot fire conditions.

Studies using water (H_2O) as the LOX simulant and nitrogen (N_2) as the fuel simulant have been conducted at both ambient and elevated chamber pressures, for example Strakey et. al[2,3] These studies can often yield a great deal of information about the atomization and mixing characteristics of a particular type of injector. As combustion chamber pressures increase, one disadvantage of studies with H_2O and N_2 is the effect of the multi-species mixtures on the thermodynamic critical properties of system. The critical properties of a mixture vary with the composition, see Davis[4], and then consequently vary both spatially and temporally in the flow field. For example, water has critical pressure of 22.06 MPa, and mixtures of N_2 with H_2O may have mixture critical pressures many times higher than this value, according to the equation of state calculations made with a modified form of Redlich – Kwong – Soave[5]. Also, $H_2O – N_2$ studies lack simulating the heat transfer processes which occur both inside and outside the injectors in a real cryogenic rocket engine. Additionally, many systems do not possess the capabilities to acoustically excite the injector flow externally. Acoustical excitations are typically observed under hot-fire conditions and can be amplified and lead into combustion instabilities and eventual loss of engine.

Investigations targeted at fundamentally understanding the injection processes and combustion stability, although ideally desirable to perform in a full-scale engine, are practically problematic and costly for many reasons, including the need for an optically-accessible full scale liquid rocket engine, special material choices, and optical diagnostic limitations. A single-element non-combusting test rig having as much of the key features of a real cryogenic rocket engine as possible, such as, cryogenic temperatures, transcritical temperature ranges, supercritical pressures, realistic

1

velocity ratios, and activation of an acoustical field inside its test chamber, is as close as one can get to the actual engine, yet avoiding indicated complications associated with the combustion in a full-scale setup. Think the test rig used in this study has such desirable characteristics. Combination of the cryogenic liquid N_2 and gaseous N_2 (to eliminate mixture critical phenomena), and N_2 – helium (He) system, to better simulate the LOX – H_2 injection issues, are available.

EXPERIMENTAL SETUP

The experimental facility, as described in detail by *Chehroudi e.t al.*[6,7], cools and liquefies (if at subcritical pressures) high pressure gaseous nitrogen (GN_2) via a heat exchanger utilizing a relatively low pressure (~0.15 MPa) liquid nitrogen (LN_2) as the cooling fluid. The liquefied nitrogen is then fed to the inner central tube of the coaxial injector (see Figure 1). A close up view of the injector tip is shown in Figure 2. For the results reported here, the cryogenic jet is injected through a sharp-edged stainless steel inner tube having a length (L) of 50 mm and inner and outer diameters measuring $d_i = 0.508$ mm and $d_o = 1.59$ mm, respectively. The resulting L/d_i is 100, considered sufficient to ensure a fully-developed turbulent pipe flow at the exit plane. The gap width (d_g) between the inner and outer tubes, defining the annular region, was 0.415 mm. The injector had an 8% bias of the mean gap width. The inner tube was slightly recessed (about one d_i). For reference, the SSME injector has a d_i of 4.77mm and a d_g of 2.24 mm.[3] The GN_2 for the annular flow is passed through a heat exchanger (different than the one mentioned above) to lower its exit temperature from the ambient to a range of 142 K – 193 K, depending on the chamber pressure and mass flow rate of the GN_2. Then, the cooled GN_2 is split and flows into two equally-spaced inlets of the ring manifold to be equally distributed later through four 90-degree-spaced tubes into the annular region well upstream of the injector exit plane. The injector is then wrapped by an insulating PTFE (Teflon) tape to minimize heat flow into the cryogenic injector from the warm chamber environment (260 K to 280 K).

The information presented here is the continuation of our work published earlier on the coaxial injection phenomena under cryogenic conditions with and without acoustic field interaction, see *Chehroudi et al.*[6,7]

The test rig is fully instrumented to measure pressure, temperature, and mass flow rates of the injected fluids. The maximum mass flow rate for the inner liquid-like flow is about 700 mg/s. The GN_2 flow fed to the ring manifold which defines the annular flow is measured using a series of three mass flow meters with a total

maximum mass flow rate of 3 g/s. A specially-designed piezo-siren by Hersh Acoustical Engineering, Inc., capable of producing sound pressure levels (SPL) of up to 180 dB (in an impedance tube) at its resonant frequencies (lying between 1000 to 8000 Hz) and at pressures up to 2000 psi is used with a circular-to-rectangular transition coupling to bring the acoustic waves into the interaction zone inside the chamber. A model 601B1 Kistler piezoelectric-type pressure transducer is used to measure the acoustic pressure variations inside the chamber at various pressures very near the jet location. The jet is located at a pressure node or velocity antinode, of a standing wave, as indicated by the measurements with the transducer. The piezo-siren acoustic driver is able to generate between 161 to 171 db when coupled with the high-pressure chamber. Back-illumination of the jet is accomplished with diffuse light flashes (0.8 μs duration). A Nikon 50 mm to 105 mm lens is used with a high resolution (1280(H) x 1024(V) pixels in an 8.6(H)x6.9(V) mm actual sensing area with a pixel size of 6.7μm x 6.7 μm) CCD camera by the Cooke Corporation to form images of the injected jets.

EXPERIMENTAL RESULTS

To help aid in discussion and be easily able to relate them to actual injectors used in cryogenic liquid rockets, the cryogenic liquid or liquid-like flow of N_2 issuing from the inner tube will be referred to as "oxidizer" and the gas or gas-like flow of N_2 issuing from the annulus between the inner and outer tubes will be called as "fuel", even though both are N_2 and neither is a fuel nor an oxidizer. However, when referring to coaxial injectors for combustion, such as Space Shuttle Main Engine (SSME), typically the oxidizer is the liquid phase oxygen and flows from the inner tube (center post) and the fuel (H2) flows from the annulus. For reference, the critical temperatures of H_2, N_2, and O_2, are 33.2, 126.2, and 154.6K, respectively; the critical pressures of H_2, N_2, and O_2, are 1.32, 3.40, and 5.04 MPa, , respectively.

Temperature Measurements

In order to estimate the physical properties and flow velocities, exit plane temperatures are needed. Many temperature measurements at various chamber pressures, "fuel" mass flow rates, and "oxidizer" mass flow rates, were made. This was accomplished by inserting a type E exposed junction thermocouple with a bead diameter (d_{tc}) of approximately 0.4 mm into the flow in both the "oxidizer" and the "fuel" at the exit plane of the injector. The temperature measurements were performed in test runs separate from those when images were collected .

2

Accurate temperature measurements are very challenging here due to the small sizes of the d_i and d_g which are of the same order as that of d_{tc}. If d_{tc} is smaller than d_i, then a better measurement of the injector exit temperature can be made, but the momentum of the fluid can break the bead or the lead wires. Considering that the thermocouple bead diameter is about the same size as the center tube inner diameter, one expects that the thermocouple bead may be touching the walls of the tube and/or locally disturbing the flow field. This will raise a question as to what temperature the thermocouple is measuring. However, attempts in correcting the thermocouple measurements by using a commercial computational fluid dynamic code (CFD++ from Metacomp, Inc.) were unsuccessful mainly because of the limitations in the equation of states utilized in the CFD++ program. Hence, we were unable to accurately predict the physical and thermodynamic properties of the nitrogen at conditions of interest in this work. However, work is underway to incorporate such features and attempt a reasonable approach in correcting the data. Nonetheless, temperature measurements were fairly repeatable and, unless otherwise indicated, uncorrected measurements were used to analyze the data presented here. Even though the absolute magnitudes of the temperature measurements are in question here, the relative trends can be regarded as reliable because of the repeatability of the test results.

Figures 3 to 5 show the center jet (oxidizer) reduced temperature measurements (T/T_c) as a function of the normalized annular fuel mass flow rate at four different pressures and for central jet mass flow rates of about 275, 450, and 625 mg/s, respectively. The annular fuel flow rate was normalized by its maximum mass flow rate at each pressure and oxidizer mass flow rate. The curves in Figures 3 to 5 are least squares fits of Equation 1 to the raw data. Equation 1 was selected because it best fits the trends of the data in Figures 3 to 5.

$$T_r = \frac{A}{\left(\dfrac{\dot{m}_{fuel}}{\max\left(\dot{m}_{fuel}\right)} + B\right)^6} + C\,\frac{\dot{m}_{fuel}}{\max\left(\dot{m}_{fuel}\right)} + D$$

Equation (1)

Where,

$T_r = T/T_c$ the reduced temperature of the "oxidizer",

$\dot{m}_{fuel}$ is the mass flow rate of the "fuel",

$\max\left(\dot{m}_{fuel}\right)$ is the maximum "fuel" mass flow rate at a given pressure and "oxidizer" mass flow rate, and

A, B, C, and D are regression constants.

At a pressure of 1.4 MPa and at all three "oxidizer" mass flow rates, the exit temperature measurements are relatively constant. Although at chamber pressure of 1.4 MPa the "oxidizer" exit temperature is within a few Kelvins of each other, there is a slight decline in the temperature as the "fuel" mass flow rate increases from a zero value. This drop in temperature is present at all pressures and "oxidizer" mass flow rates, but becomes more pronounced at higher pressures than those seen at the 1.4 MPa chamber pressure. At the zero "fuel" flow rate, warmer chamber gases are present in the annular region of the injector causing high heat transfer to the "oxidizer" through the tube walls and hence a warmer exit temperature is measured. Note that in our setup, the "fuel" flow is passed through a heat exchanger prior to introduction to the injector manifold, lowering the "fuel" temperatures well below that of the warm chamber environment. As the "fuel" flow rate is slightly increased from the zero level, it lowers the outer wall temperature of the central tube, reducing the rate of the heat losses from the inner-tube LN2, explaining the drop in its measured temperatures.

However, as the "fuel" flow rate is increased further, the "oxidizer" exit temperature increases monotonically particularly at higher chamber pressures. For all practical purposes, we can regard the inner oxidizer temperature insensitive to changes in fuel flow rate at the lowest subcritical pressure. Also, noticeable here is the less sensitive nature of the oxidizer temperature as its flow rate is increased. This is seen in Figures 3 to 5 as the fitted curves approach one another.

Figures 6, 7, and 8 show the plots of the fuel annular-flow reduced temperature measurements versus the normalized "fuel" mass flow rate at four different chamber pressures and for "oxidizer" mass flow rates of about 275, 450, and 625 mg/s, respectively. The normalization of the "fuel" mass flow rate was done the same manner as that of the "oxidizer" temperature plots presented earlier. The data were curve-fitted to a third order polynomial at each pressure and "oxidizer" mass flow rate. Exceptions to this rule are the data for the oxidizer mass flow rate of 450 mg/s (at 2.4 and 3.5 MPa) and 625 mg/s (at 2.4 and 3.5 MPa). The data for these cases were combined for curve-fitting purposes. The lumping of the data was done because of the limited amount of data at these conditions and the realization of the fact that they are very close to each other with no identifiable trend.

American Institute of Aeronautics and Astronautics

As shown in Figures 6 to 8, the measured "fuel" exit temperature never goes below the critical temperature. There is a general trend for all the cases in these figures characterized by a decline of the temperature to a minimum and a gradual rise as the fuel flow rate is increased. This appears to be a manifestation of the improved GN2 heat exchanger performance at low end and decreased residence time at the high end of the flow range investigated here. At supercritical chamber pressures, the "fuel" temperatures are generally higher than those at the subcritical and near –critical chamber pressures. However, this difference is largely reduced at the higher mass flow rates. In the middle of the "fuel" mass flow rate range, the "fuel" temperatures approaches to within 10% above the critical temperature of the nitrogen used in this study.

The temperature curve fits developed so far are convenient tools to compute differential fuel and oxidizer temperatures ("fuel" – "oxidizer"). Results are shown in Figures 9 to 11. Due to a much stronger variations of the fuel temperature with fuel mass flow rate as compared to similar changes in oxidizer temperature, the shape of the differential temperature is dictated by the annular-flow fuel temperature variations.

Using the equations of the curves fitted to the raw data, the chamber pressure measurements, and mass flow rates, densities and speed of sound of the fluids exiting the injector were computed using NIST 12 equations of state.[8] Viscosity and the thermal conductivity were calculated using the methods described in *Reid et al.*[9]

The computed fuel-to-oxidizer velocity ratios, used by some authors for assessment of possible combustion instabilities, are plotted versus chamber pressure in Figure 12. The diamond symbols in Figure 12 are the uncorrected raw data from the curve fits. The square symbols in Figure 12, are corrected "oxidizer" temperatures based on the assumption that the thermocouple measures the bulk mix mean temperature of a turbulent pipe flow, the corrected "oxidizer" temperature is what the centerline temperature would be based the turbulent pipe flow. The average correction was about 7 K. The lowering of the "oxidizer" temperature by about 7 K also agreed physically with the images taken at subcritical chamber pressures, in which the core of the jet appeared to be liquid. The uncorrected "oxidizer" temperature measurements produced densities that were on the vapor side of the saturation curve, this because at the slightly higher, uncorrected, "oxidizer" temperatures the vapor pressure is greater than the chamber pressure. At supercritical chamber pressures very little difference in uncorrected and corrected velocity ratio is evident.

Operating Conditions

The experimental matrix for the image data consisted of four different chamber pressures (~1.4, 2.4, 3.5, and 4.8 MPa), three "oxidizer" mass flow rates (~275, 450, and 625 mg/s), and five "fuel" flow rates (~0, 450, 1300, 2200, and 2800 mg/s), with the acoustic field on (at 2700 Hz) and off at each condition. Several conditions were repeated to build confidence and check the repeatability, and ten images were taken at each condition bringing the total number of images to greater than about 1400. In these tests, the "oxidizer" Reynolds numbers (Re), based on the d_i, were in the range of 1.43×10^4 to 1.88×10^5, and the "fuel" Re, based on the hydraulic diameter, d_g, reached up to 8.40×10^4. Injector exit velocity ratios ("fuel"/"oxidizer") from 0 to 35 were produced. The velocity ratios at the lowest chamber pressure reached up to about 42, whereas it approached a value near 5 at the highest pressure, see Figure 12. Note that Hulka and Hutt[1] suggested a value higher than 13 to ensure stable operation in engines utilizing coaxial injectors. However, the temperature measurements for most of the works cited therein were made well upstream of the injector exit plane and, as such, a fair comparison between the two sets of velocity ratios is not available at this time. This subject will be further investigated in our future works. There are also several factors involved in estimating velocity ratios. Our search for a better technique to make temperature measurements and/or correction logic continues to the future to provide a better estimate of this and other parameters. Also, even though the mass flow rates and the injector inner cross-section areas remained the same, the injection temperature of the "oxidizer" increased as the chamber pressure was increased (see Figures 3 to 5). Finally, the "oxidizer" temperature level in our tests are near the critical region and thus small changes in temperature (5 to 10 K) can produce large variations in the value of density, hence changing the "oxidizer" exit velocity greatly. This difficulty has also been reported by Hulka and Hutt.[1]

Image Data

A sample of the images is shown in Figure 13, and the operating conditions of the images are shown in Table 1. Images 1 to 10 are at approximately the same subcritical chamber pressure (~ 1.41 MPa), images 11 to 20 are at the same near critical pressure (~ 3.46 MPa), and images 21 to 30 are at about the same supercritical pressure (~ 4.77 MPa). The acoustic driver is off in the odd-numbered images, and on in the even-numbered images (every other row). The mass flow rate of the "oxidizer" through the inner tube is approximately the same for all the images (~ 275 mg/s) shown in Figure 13. Each column is at about a constant "fuel" mass flow rate, but increases from the left

Comment: Check with new curve fits

Comment: check

Comment: Check with new curve fits

American Institute of Aeronautics and Astronautics

column to the right. The mass flow rates of "fuel" from left to right in

Inspection of these images reveals some key features. For example, when the acoustic driver is off, the "dark core" of the jet is decreased as atomizing fuel flow rate is increased from the second column (i.e., the first non-zero fuel flow rate case) to the far right column of the images in Figure 13. The fuel flow rate plays two key roles in this injector design. First, it assists the inner jet breakup for the subcritical condition and enhances mixing for the supercritical case. Second, because of the temperature differences between the fuel and the oxidizer, there is a heat exchange between the two both inside and outside the injector. Clues for the heat transfer behavior can be taken by examination of the injector temperature measurements. For instance, as mentioned earlier it appears that at the lowest subcritical chamber pressure, the inner oxidizer jet temperature is fairly insensitive to the annular fuel flow rate. However, at all other elevated pressures, particularly at the supercritical one, a gradual increase in the oxidizer exit temperature can be detected.

The case for the zero fuel flow rate is interesting. Under this condition, the annular passage of the injector is filled with the warm chamber nitrogen, strongly affecting the heat transfer not only inside but also outside the injector. Clear evidences for the high heat transfer rate inside the injector come from the exit temperature measurements under this condition, see Figures 3 to 8. Here, the observed elevated temperature is believed to be the effects of the warm chamber gases present inside the annular space of the injector. Hence, even though no atomizing flow is at work here, one sees a shorter dark core than those seen in other images presented in the second column from the left (i.e. the lowest atomizing fuel flow rate), see Figure 13. A small flow of the colder-than-chamber fuel in the annular passage, although assists the jet breakup, lowers the oxidizer exit temperature. The two phenomena work in such a way that the net effect is an apparent longer dark core in most cases, compare the images in column one and two from the left of Figure 13. Effects of the acoustic field are discussed in the next section.

Effects of the Acoustic Field

Looking at images in Figure 13, one trend that stands out is that the coaxial jet appears to be more sensitive to the existence of the acoustic field under subcritical chamber pressure. Although the images shown in this figure are typical, we thought to devise an approach to be able to systematically assess the interaction of the jet and the acoustic field.

In order to assess the global effects of the acoustic field, each data condition was assigned an acoustic effect of 0, 1, or 2, based upon the qualitative behavior of the jet. An acoustic effect of "0" corresponds to no distinguishable effect from all the images at a given condition. For example, images 15 and 16 in Figure 13. An acoustic effect of "2" corresponds to a strong effect, such as the large-amplitude spatially-superimposed sinusoidal wave seen in images 6 and 8 as compared to images 5 and 7, respectively, or the interaction shown in images 1 and 2 in Figure 13. An acoustic effect of "1" corresponds to a weaker effect than that of a "2", but definitely present, unlike an acoustic effect of "0". An example of an acoustic effect of "1" is the small amplitude sinusoidal wave of image 12 as compared to image 11 and the contraction of the length of the dark core in image 24 compared to image 23 in Figure 13. For the images shown in Figure 13 the rating of the acoustic field effect is listed in Table 1.

In order to determine the effect of the flow rates (fuel/oxidizer ratio) and chamber pressure, rating of the acoustic field effects is plotted in Figure 14. It is now clear that the strongest effect of the acoustic field occurs at the lowest chamber pressure and as pressure increases towards the supercritical conditions, the observable acoustic effect diminishes. However, there are still cases that even under supercritical chamber pressures one can isolate observable effects of the acoustic field. Interestingly, there is a zone in mass flow rate ratios space, located nearly in the middle of the investigated range, in which one sees no acoustic effects even under subcritical condition, see Figure 13. For further processing of the acoustic effects, an average of all the ratings was computed at each chamber pressure, regardless of "fuel" or "oxidizer" mass flow rates, and results are plotted versus chamber pressure in Figure 15. The plot shows that, on the average as the chamber pressure increases to the critical pressure value, the effect of the acoustic field decreases. Interestingly, near the critical pressure and beyond into the supercritical regime, the acoustic field has minimal effect on the coaxial injector flow dynamics.

Obviously, the jet behaves differently at different "fuel" mass flow rates. Recall that the fuel mass flow rate acts as the atomizing gas, accelerating the breakup mechanism. At the lowest subcritical chamber pressure, for the case of a single inner-tube jet (i.e., zero "fuel" mass flow rate), comparing images 1 and 2 (Figure 13) the acoustic field shatters the jet into many droplets and ligaments, causing accelerated jet breakup. As the mass flow rate of the "fuel" increases slightly (~ 487 mg/s), such as images 3 and 4 (Figure 13), the "oxidizer" begins to break up into relatively large droplets and ligaments as a result of the atomizing "fuel" flow. The droplets and ligaments, which have a slightly higher

5

density at these conditions, see exit temperature measurements at the lowest subcritical pressure, consequently have a higher momentum, and thus acoustic field has somewhat of a lesser effect. Note that from our previous measurements, the jet is located at the pressure node or velocity antinode. As the "fuel" flow rate increases even more, finer droplets and ligaments are formed from the "oxidizer", and more of its mass from the intact core is converted into droplets and ligaments. This consequently produces a shorter and less dark core for the oxidizer jet. Additionally, as the "fuel" flow rate increases, the heat transfer from the "fuel" to the "oxidizer" increases outside the injector, lowering the average density of the oxidizer core in the injector near field area. Under the subcritical condition, this combined annular fuel-flow-enhanced atomization and heat transfer creates a dark core region more susceptible to the acoustic field, see Figures 6 to 8.

As the pressure increases to a near-critical value (images 11 to 20, Figure 13) droplets are no longer evident as the surface tension approaches zero. Examination of many images including those shown in Figure 13 indicates that the acoustic effects are substantially reduced and hardly noticeable. A weak sinusoidal wave is visible superimposed on the jet when the acoustic driver is turned on under the zero "fuel" mass flow rate condition and at near-critical chamber pressure (see images 11 and 12 in Figure 13). However, at the higher atomizing "fuel" mass flow rates, no distinguishable effect of the acoustic field is observed (see images 15 through 20 in Figure 13). Similarly, at supercritical chamber pressures (images 21 through 30, Figure 13), only minor effects of the acoustic field are observed at the lowest nonzero "fuel" flow rate conditions. This, although unclear in images 23 and 24 of Figure 13, but was evident when all the 20 images at these two particular conditions were studied. Acoustic field effects are even weaker at higher atomizing "fuel" flow rates, see image pairs (25, 26), (27, 28), and (29, 30).

It is thought that acoustic impedance of the jet core may play a role in what is observed here. Hence, a phase diagram was created to map the characteristic acoustic impedance, i.e., product of the density and speed of sound (ρc) at the injector exit plane conditions, and is shown in Figure 16. The data conditions in this figure are corrected based upon the assumption that the flow approaching the thermocouple beads has a turbulent profile and that the thermocouple measures a mixed-mean temperature. The correction methodology attempts to estimate the value of temperature at the center of the profile. This correction logic was applied only for the subcritical pressures for the following reason. At first attempt the uncorrected raw data was

plotted and we found that at subcritical chamber pressures, the raw data fell on the vapor side of the saturation curve. After this correction was applied only one point remained on the vapor side of the saturation curve. This was due to the fact that the chamber pressure was lower than the saturation pressure at the measured inner tube "oxidizer" temperature values, thus suggesting a vapor state from the equilibrium thermodynamics considerations. However, the magnified images at these subcritical conditions strongly suggested that the center jet ("oxidizer") goes through the classical liquid-phase breakup processes at these conditions. Therefore, it was deemed necessary to provide the best temperature correction available at present time (described earlier) to preserve a physically consistent picture between evidences from the acquired images and temperature measurements. We continue exploring better measurement techniques and correction methodologies for a more accurate determination of the injector exit plane temperature. The characteristic acoustic impedance of the "oxidizer" is the highest at subcritical pressures.

One may theorize that the larger the differences between the acoustic impedance (ρc) for the "oxidizer" with respect to the warm chamber environment gases (particularly for the dark core zone) the greater the effects of the acoustic field would be on the jet. Figure 16 shows that amongst the cases where strong acoustic effects were observed (i.e. diamond symbol), a large majority (10 out of 12, not counting the subcritical pressure point on the vapor side of the saturation curve) of them have high acoustic impedance and exist under subcritical chamber pressure. Conversely, good majorities (21 out of 32) of those that exhibit no acoustic effect (i.e. square symbol) have low acoustic impedance and exist under supercritical chamber pressure. However, there are still some cases where despite their high impedances, are apparently insensitive to the acoustic field, (see all the square symbols at and below 2.5 MPa in Figure 16).

Figure 17 shows coaxial instability data for actual engines reported in Hulka and Hutt.[1] Superimposed on these results are velocity ratios from our injector. Based on a large set of data from both stable and unstable engine operation, they offered a triangular zone beyond which most engines were stable. In fact, they suggested that as long as the injector velocity ratio is above a number of 13, the engine would highly likely be stable. It was unclear, however, what the underlying physical reasons were. Looking at our data in Figure 17, it is apparent that it tells a different story. That is, whenever we rate the injector to be minimally sensitive to the acoustic field, such as supercritical condition, the velocity ratio is low and buried into the triangular zone

6

Hulka and Hutt[1] consider as unstable engine operation. The temperature measurements made in our work were made at the injector exit plane. It is unclear where the temperature measurements were made in the real rocket engine conditions (probably upstream of the injector exit plane) presented by Hulka and Hutt[1]. This matter becomes even more important near the critical point as small changes in temperature leads to large variations in density and velocity ratio calculations. Therefore, some caution must be used at this point before making one to one comparisons. However, we feel that these initial data have a good degree of relevancy to actual engines. Primarily, we have some initial clues because of our unique setup, being able to span subcritical to supercritical chamber pressures, cryogenic fluid simulant, and coaxial injector bearing major features of the production ones.

To offer a perspective, although not complete and evolving, we would like to propose a hypothesis based on our evidences here and other researchers, Oefelien and Yang[10], who reported that an acoustically-established crossflow interaction with the jet is one important parameter playing a role in engine stability. We have two choices to formulate this hypothesis and to connect what is observed here to the actual engine combustion instability. Intuitively, one can assume that the coaxial jet we observe and rate here as sensitive to the acoustic field leads to an engine instability when carried into an actual engine. In other words, the assumption is that the jet characteristics (visual and nonvisual) which make our coaxial injector highly sensitive to the acoustic field also are responsible for the observed engine instability. The reason this is a possibility comes from the fact that engines become stable when hydrogen fuel temperature is raised beyond a threshold value. One would expect that the heat transfer at higher temperatures tends to "shorten and thin" the jet core region, similar to what is observed here, particularly at supercritical pressures when the jet in our facility becomes insensitive to the external acoustic field. On the other hand, factors responsible for a most sensitive injector in our rig may actually be stabilizing agents in actual engines. The argument in favor of this case comes from the fact that in an actual engine the existence of the mixing critical temperature and pressure in the mixing layer can create a jet core similar to what is observed in our most sensitive cases (such as those under subcritical condition). Although this latter hypothesis is aligned with the Hulka and Hutt[1] data in Figure 17, the former appears more intuitive. Certainly, more work is needed to establish this important connection between our measurements and the engine combustion instability.

A comment regarding Figure 17 is necessary here. Note that although Hulka and Hutt[1] present their stability data in a form of the velocity ratio, what usually used for stability rating is the so-called "temperature ramping". This means that there is a threshold minimum fuel (hydrogen) temperature above which engine has shown stable operation. It appears that one important phenomenon at play with the coaxial injectors is the heat transfer, both inside the injector element and in the mixing layer between the central "oxidizer" jet and the annular "fuel" flow in the chamber. This phenomenon is fairly complex especially under supercritical chamber conditions. What we think acting here is the combination of the characteristic acoustic impedance and the momentum of the jets. Obviously, it is the temperature of the fuel and, in effect, the nature of the heat transfer (both inside and immediately outside of the injector) that affects both factors particularly at near- and supercritical conditions. Note that our temperature measurements in Figures 3 to 5 show that at subcritical temperatures the oxygen exit temperature is unaffected by the nature of the heat transfer inside the injector. However, this is not the case for the supercritical condition.

Figure 18 shows a plot of the fuel/oxidizer momentum ratio as a function of the fuel/ambient characteristic acoustic impedance ratio. Note that how our data at different chamber pressures are separated in this diagram. If one defines a region where most of the cases with acoustic interaction rating of 2 lie, and likewise the same for those with rating of zero, one will see two separated zones with some overlap region. Although data is scarce, it suggests that when both momentum ratio and the acoustic impedance of the jet are high, one should expect maximum interaction between the jet and the acoustic field and vice versa.

Although we do not yet have a fully coherent picture, we feel that both the acoustic impedance (see Figures 16 and 18) and the momentum of the jet create a condition under which the coaxial jet becomes highly sensitive to the acoustic field disturbances. In fact, at first glance, it is possible that as temperature is ramped up in a production engine for stability analysis, strong heat transfer, both inside and immediately outside the injector, "shortens" and "thins" the oxidizer core in a manner similar to what is observed in image pairs of (7 and 27) or (9 and 29) to make it insensitive to the acoustic field that is established inside the combustion chamber.

SUMMARY AND CONCLUSIONS

Temperature measurements were made at the exit plane of a model of the coaxial injectors used in cryogenic rocket engines. The trends should be viewed specific to our facility unless it is verified for practical engines. Everything else being the same, the results of the

7

temperature measurements showed that as the chamber pressure increases the center jet ("oxidizer") temperature increases. The mass flow rate of the "fuel" in the annular passage of the injector has a stronger effect on both the "fuel" and the "oxidizer" exit temperatures than the "oxidizer" mass flow rate. As the "fuel" mass flow rate increases from zero, both the "fuel" and "oxidizer" temperatures first decrease, reach a minimum, but at different flow rates, somewhere in the middle of the "fuel" mass flow range, and then increase again. Due to measurement difficulties in very small passages, the magnitudes of the actual temperatures are not yet known with great accuracies. However, their trends with pressure and mass flow rate can be regarded as valid.

Back-lit images of the coaxial jet were taken at four chamber pressures, three "oxidizer" mass flow rates, and five "fuel" flow rates with a 2700 Hz external acoustic field turned either on or off. Preliminary analysis of the data shows that the effects of the acoustic field was more noticeable at subcritical chamber pressures where the jet behaved liquid-like and had high characteristic acoustic impedance. For the most part, the coaxial jet became insensitive to the external acoustic field under supercritical conditions where the dark central core of the jet became short and "thin". Under this condition, the characteristic acoustic impedances are generally lower than those under subcritical conditions.

We postulated that the sensitivity characteristics of the coaxial jet to the external acoustic field in our setup may correspond to that causing combustion instability in engines. However, exact nature of this connection is to be further investigated. Stronger effects of the acoustic field on the coaxial jet were evident at higher velocity ratios (> 10) whereas weaker interactions were seen at lower velocity ratios (< 10). Although Fuel/oxidizer velocity ratio is used as one parameter for characterization of the engine instability, we felt to search for a different set of parameters to physically represent our data. It is proposed that fuel/oxidizer momentum ratio and an acoustic parameter, such as characteristic acoustic impedance, be used. That the characteristic acoustic impedance of the central "oxidizer" jet plays a role and ultimately a parameter to be considered in engine stability studies remain to be further studied through more data and analysis. Preliminary evidences from the data presented here are pointing in that direction.

ACKNOWLEDGEMENT

REFERENCES

1. Hulka, J. and Hutt, J.J. *Instability Phenomena in Liquid Oxygen/Hydrogen Propellant Rocket Engines*, in *Liquid Rocket Engine Combustion Stability*, V. Yang and W. Anderson, Editors. 1994, AIAA: Washington. p. 39-71.

2. Strakey, P.A., Talley, D.G., and Hutt, J.J. *Mixing Characteristics of Coaxial Injectors at High Gas/Liquid Momentum Ratios*. Journal of Propulsion and Power, 2001. 17(2): p. 402-410.

3. Strakey, P.A., et al. *Effects of Liquid-Oxygen Post Biasing on SSME Injector Wall Compatibility*. Journal of Propulsion and Power, 2002. 18(2): p. 240-246.

4. Davis, D. *Supercritical Fuel Injection Studies for Advanced Gas Turbine Engines*, M.S. Thesis, *Mechanical Engineering*. 2001, The Pennsylvania State University: University Park. p. 103.

5. API, *Technical Data Book - Petroleum Refining*. Sixth Ed., Thirteenth Revision Package ed, ed. T.E. Daubert and R.P. Danner. 1999, Washington: American Petroleum Institute.

6. Chehroudi, B. and Talley, D. *Interaction of Acoustic Waves with a Cryogenic Nitrogen Jet at Sub- and Supercritical Pressures*. in *40th AIAA Aerospace Sciences Meeting and Exhibit*. 2002. Reno, NV.

7. Chehroudi, B., Davis, D., and Talley, D. *Initial Results From A Cryogenic Coaxial Injector In An Acoustic Field*. in *41th AIAA Aerospace Sciences Meeting & Exhibit*. 2003. Reno, Nevada.

8. Lemmon, E.W., et al. *NIST 12 Thermodynamic and Transport properties of Pure Fluids*. 2000, U. S. Secretary of Commerce.

9. Reid, R.C., Prausnitz, J.M., and Poling, B.E. *The Properties of Gases and Liquids*. 4th ed. 1987, New York: McGraw-Hill. 741.

10. Oefelien, J.C. and Yang, V. *Comprehensive Review of Liquid Propellant Combustion Instabilities in F-1 Engines*. Journal of Propulsion and Power, 1993. 9(5): p. 657-677.
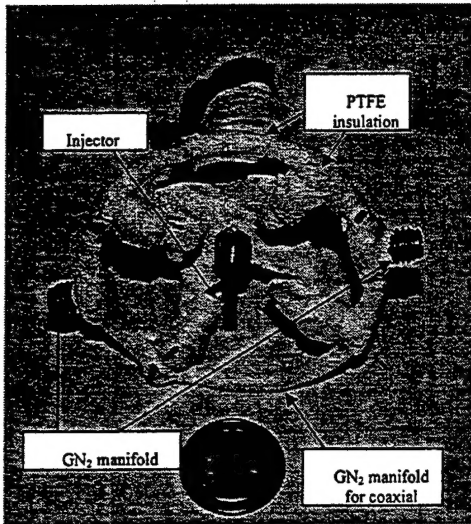
Figure 1 Picture of the coaxial injector.

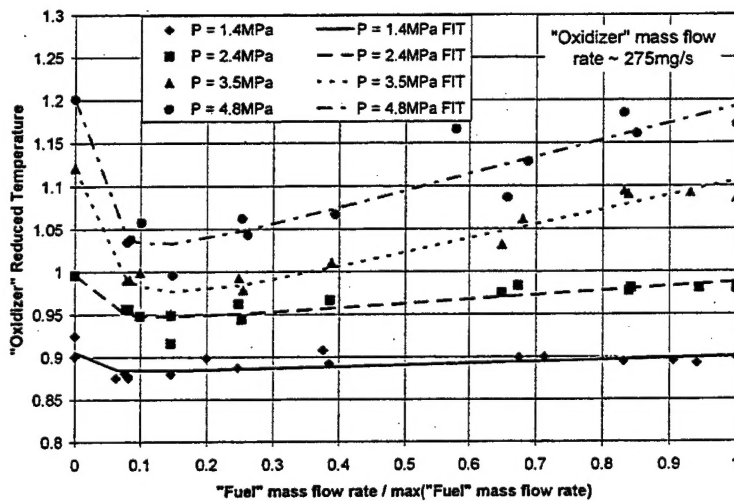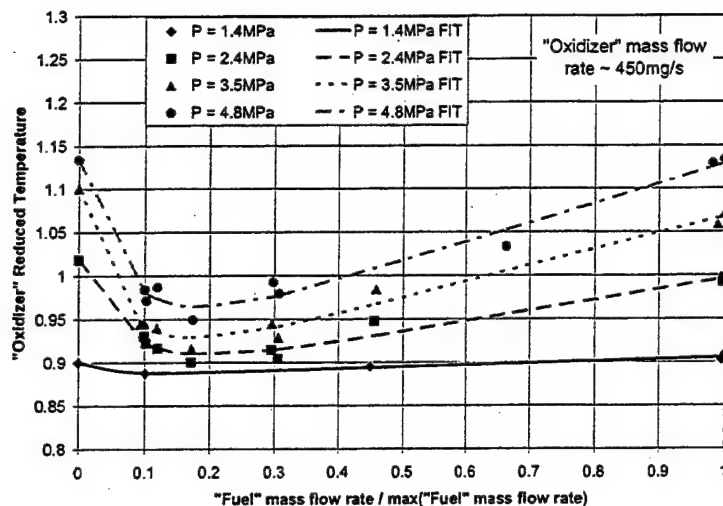Figure 2 Close up view of the coaxial injector tip.

Figure 3 The center jet ("oxidizer") reduced temperature versus the annular flow ("fuel") mass flow rate normalized by the maximum "fuel" mass flow rate at four different chamber pressures. Oxidizer mass flow rate is fixed at about 275 mg/s. The lines, called "FIT" on the inset, are curve fits to the raw data. The maximum "fuel" mass flow rates for 1.4, 2.4, 3.5, and 4.8 MPa are 2995, 2985, 2974, 2918 mg/s, respectively.

American Institute of Aeronautics and Astronautics

Figure 4 The center jet ("oxidizer") reduced temperature versus the annular flow ("fuel") mass flow rate normalized by the maximum "fuel" mass flow rate at four different chamber pressures. Oxidizer mass flow rate is fixed at about 450 mg/s. The lines, called "FIT" on the inset, are curve fits to the raw data. The maximum "fuel" mass flow rates for 1.4, 2.4, 3.5, and 4.8 MPa are 2535, 2513, 2511, 2485 mg/s, respectively.
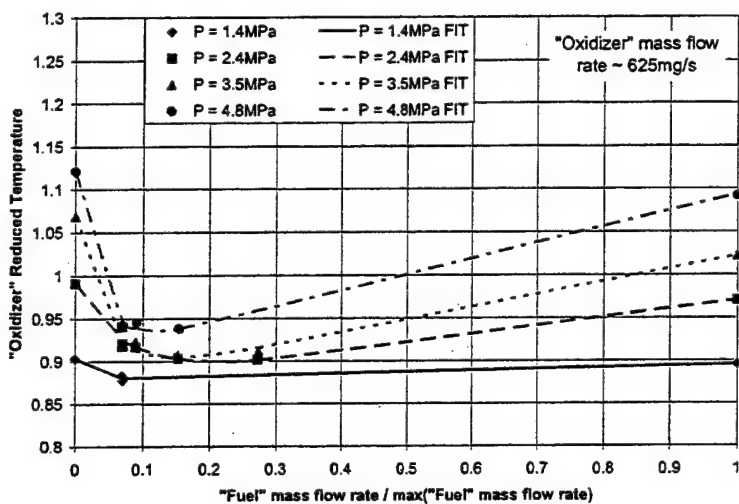

Figure 5 The center jet ("oxidizer") reduced temperature versus the annular flow ("fuel") mass flow rate normalized by the maximum "fuel" mass flow rate at four different chamber pressures. Oxidizer mass flow rate is fixed at about 635 mg/s. The lines, called "FIT" on the inset, are curve fits to the raw data. The maximum "fuel" mass flow rates for 1.4, 2.4, 3.5, and 4.8 MPa are 2814, 2821, 2805, 2757 mg/s, respectively.
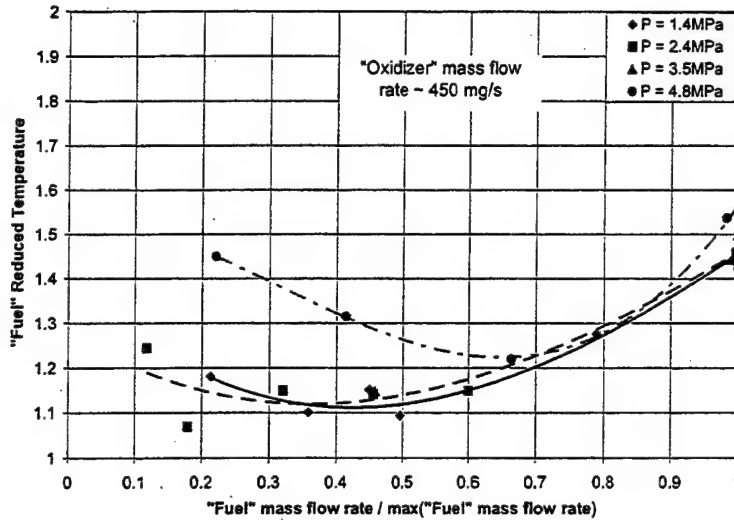
American Institute of Aeronautics and Astronautics

Figure 6 · The annular flow ("fuel") reduced temperature versus the normalized "fuel" mass flow rate at four different chamber pressures. Oxidizer mass flow rate is fixed at about 275 mg/s. The lines are curve fits to the raw data. The maximum "fuel" mass flow rates for 1.4, 2.4, 3.5, and 4.8 MPa are 2995, 2985, 2974, 2918 mg/s, respectively.
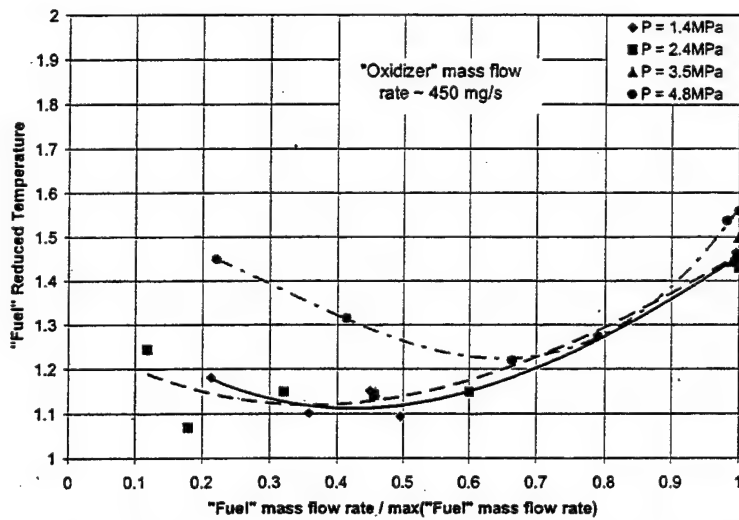

Figure 7 The annular flow ("fuel") reduced temperature versus the normalized "fuel" mass flow rate at four different chamber pressures. Oxidizer mass flow rate is fixed at about 450 mg/s. The lines are curve fits to the raw data. Data for the chamber pressures of 2.4 and 3.5 MPa are combined for curve fitting. The maximum "fuel" mass flow rates for 1.4, 2.4, 3.5, and 4.8 MPa are 2535, 2513, 2513, 2485 mg/s, respectively.
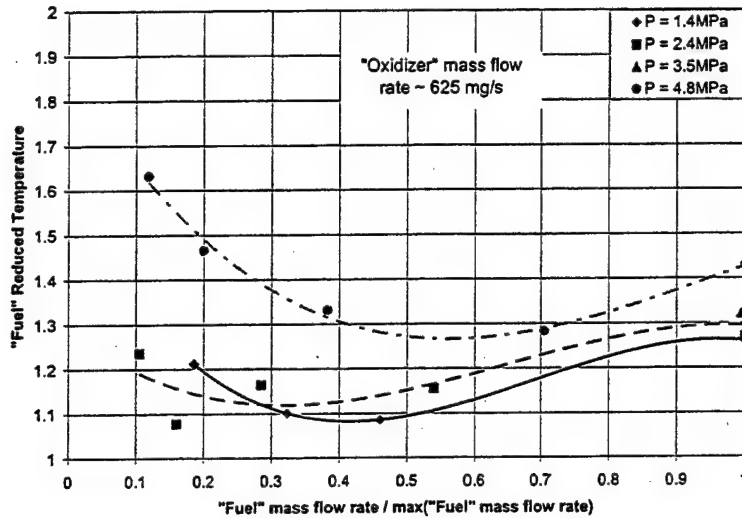
American Institute of Aeronautics and Astronautics

Figure 8 The annular flow ("fuel") reduced temperature versus the normalized "fuel" mass flow rate at four different chamber pressures. Oxidizer mass flow rate is fixed at about 625 mg/s. The lines are curve fits to the raw data. Data for the chamber pressures of 2.4 and 3.5 MPa are combined for curve fitting. The maximum "fuel" mass flow rates for 1.4, 2.4, 3.5, and 4.8 MPa are 2814, 2821, 2821, 2757 mg/s, respectively.
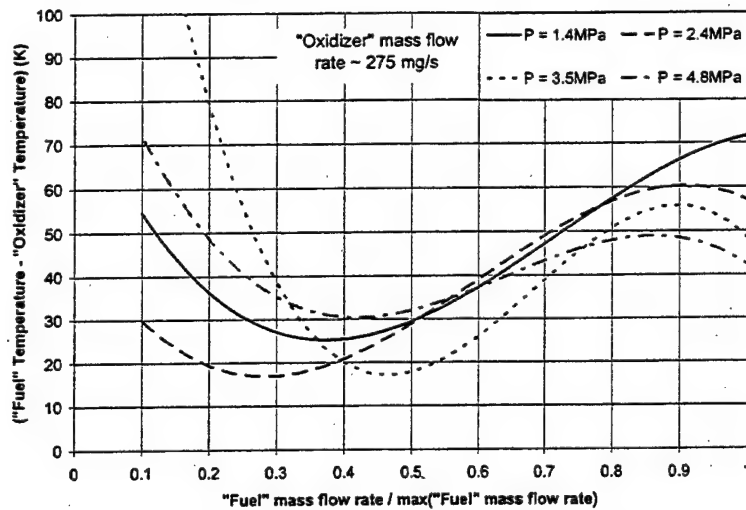

Figure 9 Differential temperature ("fuel" –"oxidizer") for four different chamber pressures, at an "oxidizer" mass flow rate of about 275 mg/s.
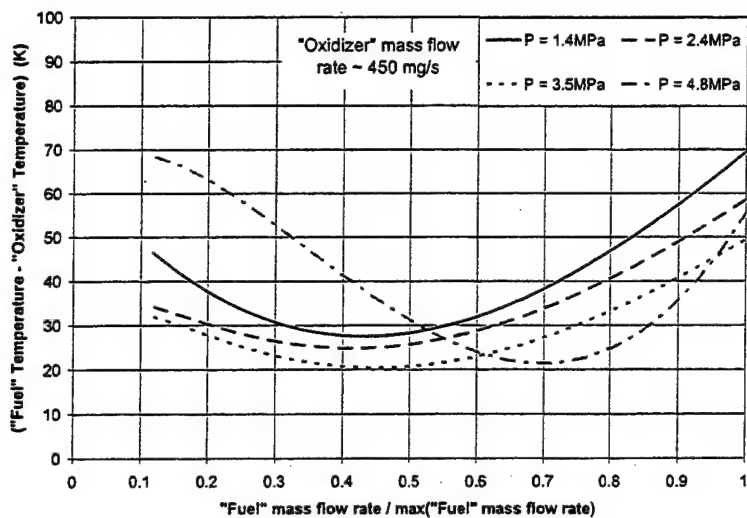
12

American Institute of Aeronautics and Astronautics

Figure 10. Differential temperature ("fuel" –"oxidizer") for four different chamber pressures, at an "oxidizer" mass flow rate of about 450 mg/s.
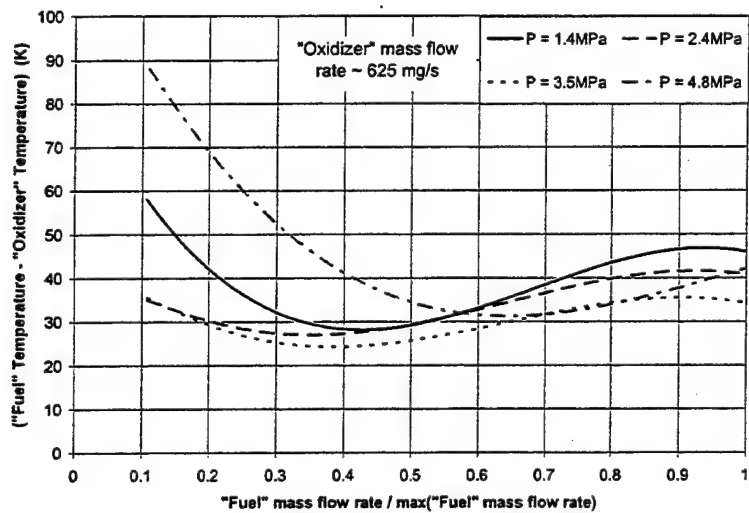

Figure 11 Differential temperature ("fuel" –"oxidizer") for four different chamber pressures, at an "oxidizer" mass flow rate of about 625 mg/s.
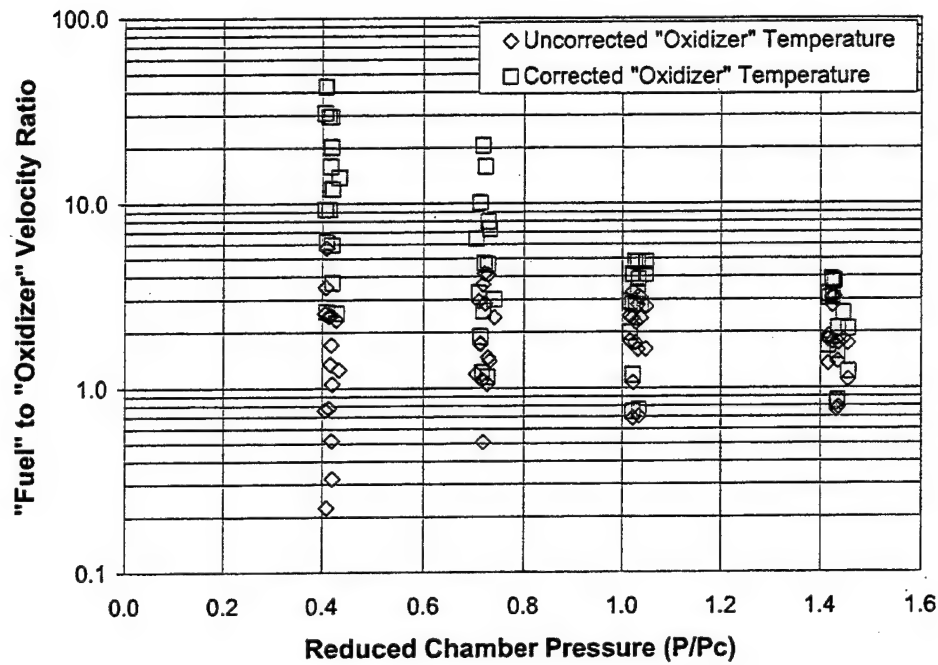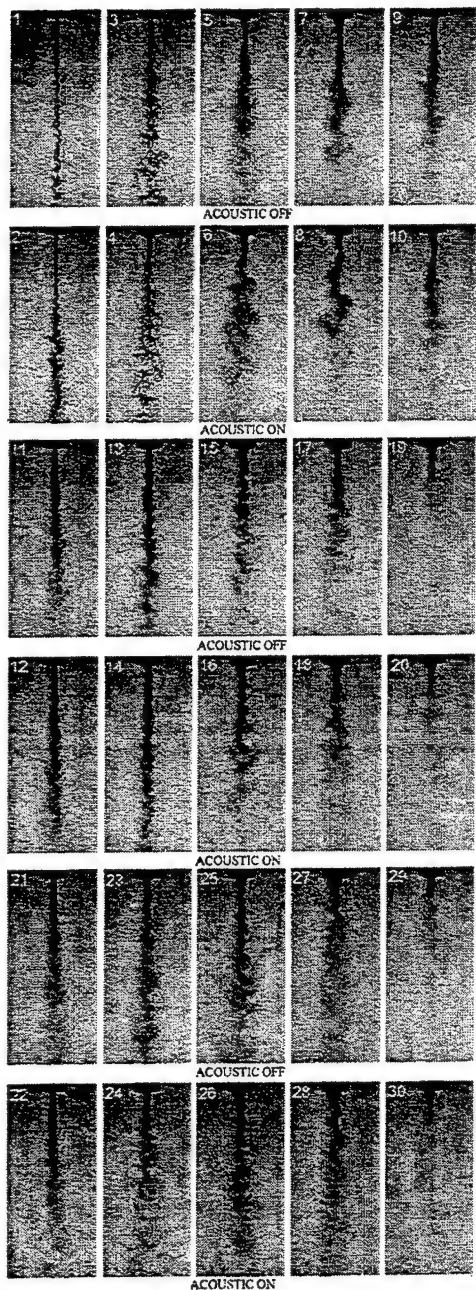
Figure 12 "Fuel" / "Oxidizer" Injection velocity ratio variation over the pressure range of the tested conditions. Corected "oxidizer" temperature was lower by about 7K. Critical pressure of nitrogen is 3.4 MPa.

American Institute of Aeronautics and Astronautics

"fuel" mass flow rates passing through the annulus. For each row, the "fuel" mass flow rate starts at a zero value and increases from the left column to the right. The acoustic driver is off/on for the odd/even numbered jet images, respectively. The chamber pressure levels for images 1-10 are subcritical, for 11-20 are near-critical, and for 21-30 are supercritical. The data conditions are shown in Table 1 of the Appendix.

Figure 13. Images of the coaxial jet at approximately the same "oxidizer" mass flow rates through the inner tube (~ 275 mg/s). Columns are at about the same

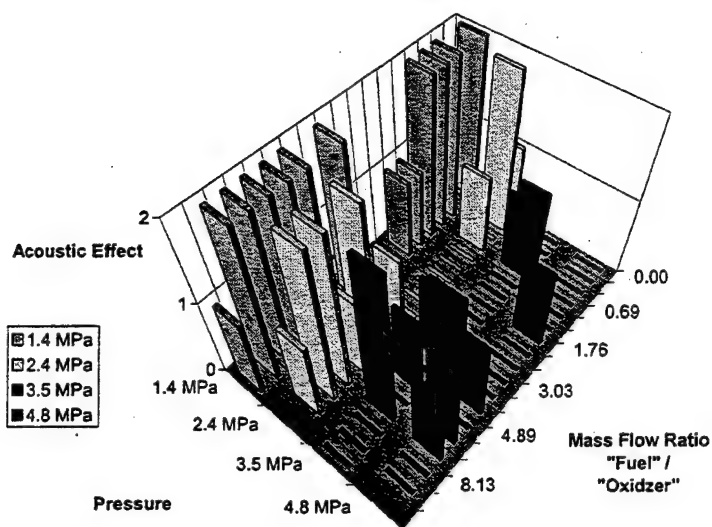American Institute of Aeronautics and Astronautics

Figure 14 Changes in the rating of the acoustic field effects with variations of the chamber pressure and "fuel" / "oxidizer" mass flow rate ratio. Critical pressure of nitrogen is 3.4 MPa.

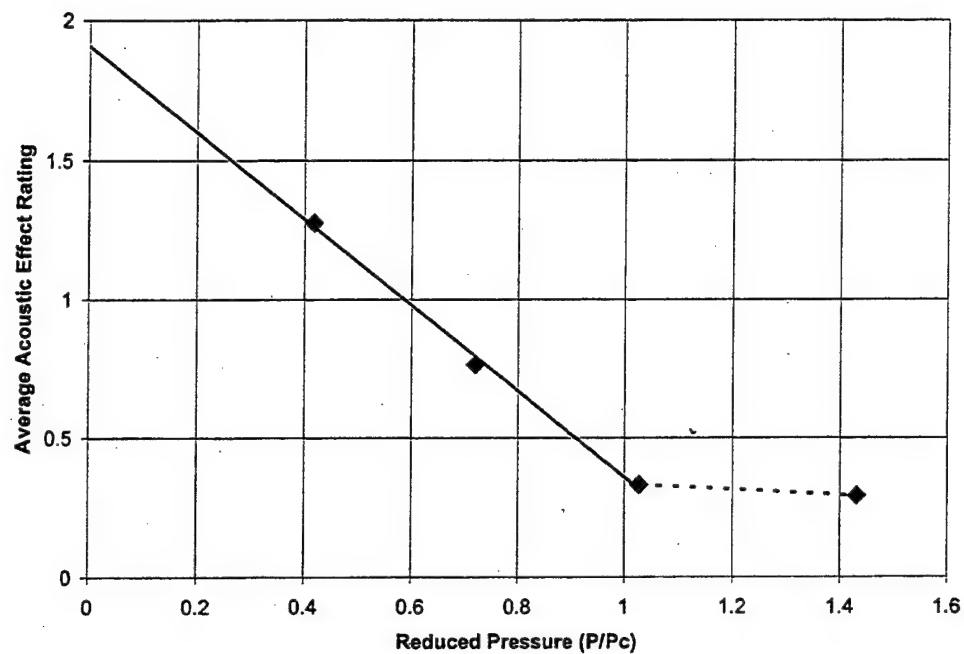American Institute of Aeronautics and Astronautics

Figure 15 Averaged acoustic effect rating as a function of the reduced chamber pressure. At each pressure, averaging is done over all the fuel/oxidizer mass ratios shown in Figure 14.

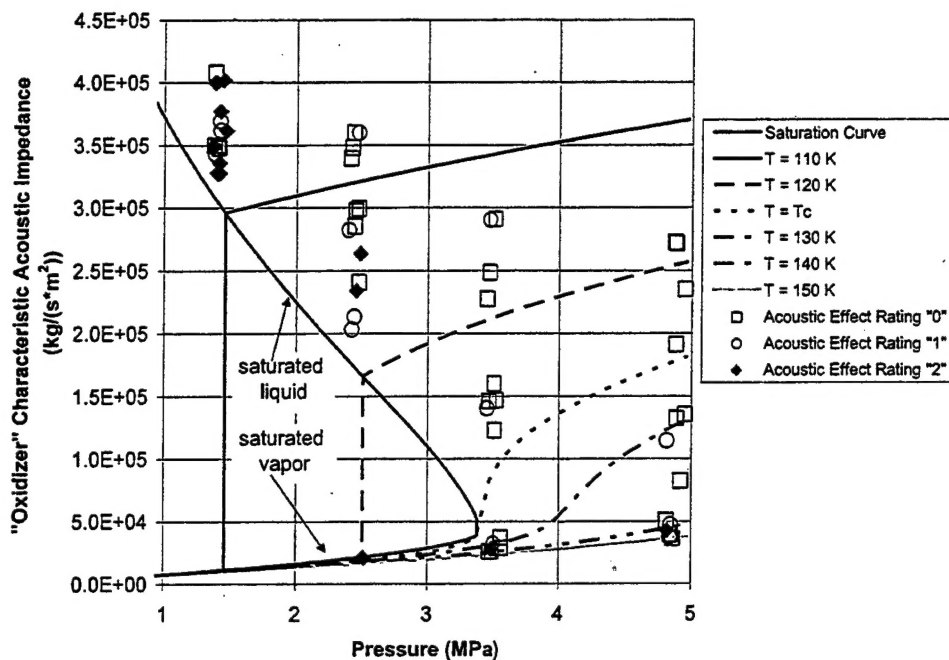American Institute of Aeronautics and Astronautics

Figure 16 Phase diagram of the calculated characteristic acoustic impedance at the injector exit plane for the "oxidizer". Note that the present data was corrected at subcritical chamber pressures.
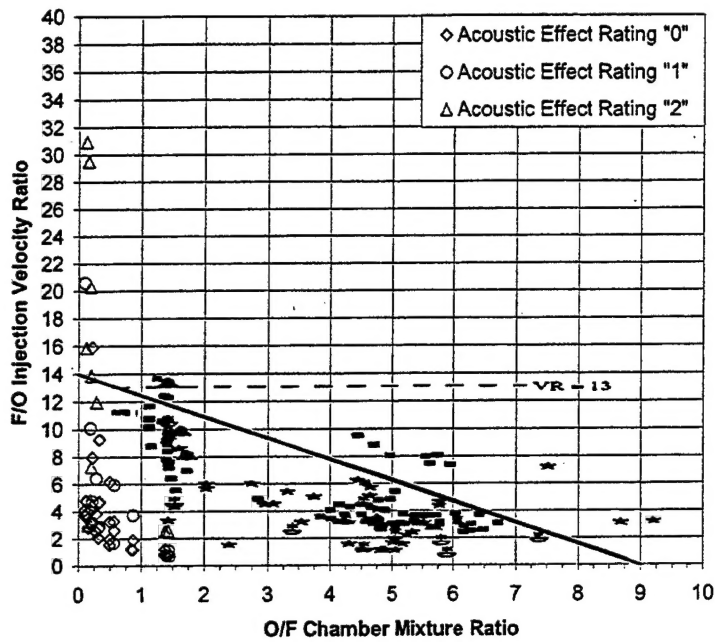
Figure 17. Coaxial injector instability zone by Hulka and Hutt[1], indicting a triangular zone in which most of the unstable engine operation was observed. The hollow diamond, hollow up-triangle, and hollow circle show results from the injector used in this study, the solid points are from Hulka and Hutt.[1]

American Institute of Aeronautics and Astronautics

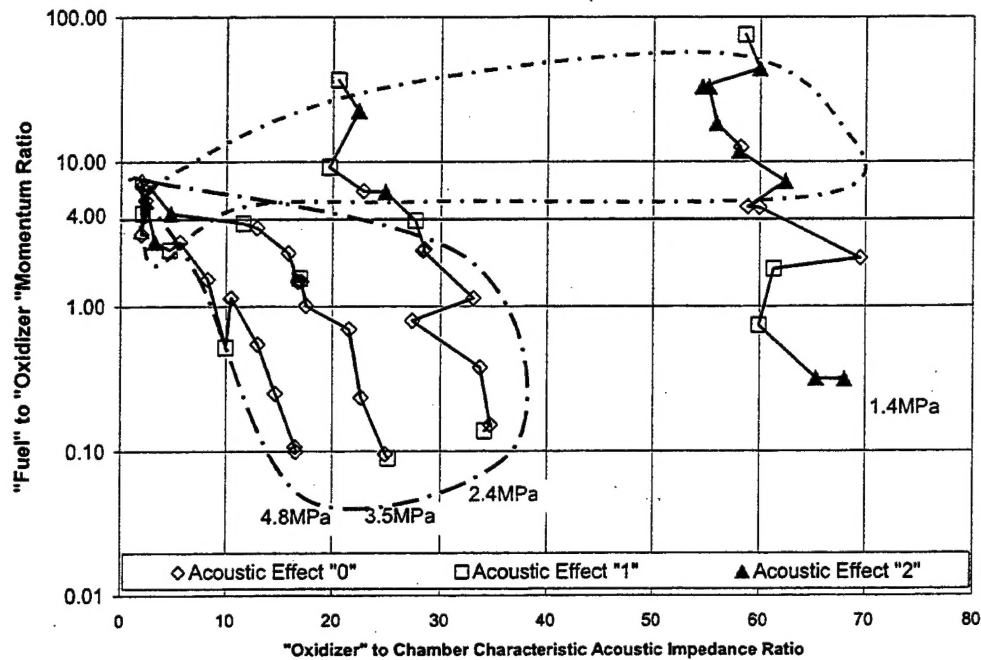Figure 18 Shows the fuel/oxidizer momentum ratio as a function of the acoustic impedance ratio for all the conditions tested. Different symbols indicate our acoustic-jet interaction ratings. The dashed curve attempts to enclose most of the up-triangle symbol and dash-dot curve does the same for the diamond. The single hollow up-triangle is at 2.4 MPa and is on the vapor side of saturation curve at the predicted temperature.

TABLE

Table 1. Conditions at which the jet images shown in Figure 13 are taken.

Jet Number	Acoustic Field	Chamber Pressure	Exit Temperature "Fuel"	Exit Temperature "Oxidizer"	Mass Flow Rate "Fuel"	Mass Flow Rate "Oxidizer"	Re "Fuel"	Re "Oxidizer"	Acoustic Effect
-	-	MPa	K	K	mg/s	mg/s	-	-	-
1	off	1.36	179	114	0	276	0.00E+00	8.09E+04	2
2	on	1.36	179	114	0	276	0.00E+00	8.10E+04	2
3	off	1.44	146	112	488	276	1.67E+04	8.14E+04	1
4	on	1.40	146	112	486	276	1.67E+04	8.18E+04	1
5	off	1.47	144	112	1360	276	4.69E+04	8.08E+04	2
6	on	1.45	144	112	1354	277	4.68E+04	8.12E+04	2
7	off	1.49	173	-113	2255	277	6.71E+04	8.06E+04	2
8	on	1.35	173	113	2255	277	6.74E+04	8.17E+04	2
9	off	1.38	182	114	2812	278	8.08E+04	8.15E+04	1
10	on	1.36	182	114	2820	278	8.10E+04	8.16E+04	1
11	off	3.47	179	138	0	275	0.00E+00	5.83E+04	1
12	on	3.52	179	138	0	275	0.00E+00	5.79E+04	1
13	off	3.47	146	119	488	275	1.47E+04	1.49E+04	0
14	on	3.44	146	119	489	275	1.48E+04	1.49E+04	0
15	off	3.45	144	126	1362	275	4.12E+04	1.97E+04	0
16	on	3.50	144	126	1355	276	4.08E+04	1.95E+04	0
17	off	3.51	173	133	2255	276	6.29E+04	5.59E+04	0
18	on	3.50	173	133	2254	276	6.29E+04	5.61E+04	0
19	off	3.37	182	137	2836	277	7.73E+04	5.95E+04	0
20	on	3.41	182	137	2835	276	7.71E+04	5.89E+04	0
21	off	4.74	245	144	0	271	0.00E+00	4.81E+04	0
22	on	4.90	245	144	0	268	0.00E+00	4.62E+04	0
23	off	4.78	189	126	486	270	1.23E+04	1.56E+04	1
24	on	4.73	189	126	486	272	1.23E+04	1.58E+04	1
25	off	4.78	163	134	1363	272	3.62E+04	3.27E+04	0
26	on	4.73	163	134	1363	272	3.64E+04	3.34E+04	0
27	off	4.78	185	142	2262	270	5.78E+04	4.61E+04	0
28	on	4.76	185	142	2275	270	5.82E+04	4.65E+04	0
29	off	4.74	193	148	2835	273	7.11E+04	4.98E+04	0
30	on	4.77	193	148	2838	272	7.11E+04	4.95E+04	0

American Institute of Aeronautics and Astronautics